Marine Research
of the National Academy of Marine Research
ISSN: 2709-6629 (Vol.4 Iss.2)
GPN: 2011200033

DOI: http://dx.doi.org/10.29677/MR.202412_4(2).0002
2024, 4(2), 17-29

Study on the Maximum Power Point Tracking of a Point-absorber Wave Energy Converter

Bo-Han Wang [1] Tzu-Hung Huang [1] Yang-Chi Chung [1]
Hung-Ming Chen [1] Yu-Chi Chang [1] Wen-Yang Hsu [2*]

[1] *Green Energy and Environment Research Laboratories, Industrial Technology Research Institute, Tainan, Taiwan*

[2] *Department of Harbor and River Engineering, National Taiwan Ocean Universality, Keelung, Taiwan*

ABSTRACT

Ocean energy has been identified as an innovative energy source and is expected to play a crucial role in Taiwan's pathway to net-zero emissions by 2050. One of the challenges in developing wave energy converters (WECs) arises from the intermittency of wave energy, in which the incident wave energy can fluctuate significantly within several seconds. This study focuses on the maximum power point tracking (MPPT) of a point-absorber wave energy converter (PA-WEC) under irregular wave conditions. To assess the PA-WEC's performance under specific sea conditions, a wave-to-wire model using the ANSYS AQWA software was developed. The model integrated frequency-domain hydrodynamics and time-domain PTO damping, allowing the authors to obtain the drive rope tension, drive rope velocity, floater motion, and power output of the PA-WEC. The simulated results were further applied to design the MPPT algorithm. Large-scale physical model tests were conducted to validate the numerical model using data from irregular wave conditions in a wave flume. Both numerical simulations and experiments demonstrated that optimal PTO damping exists for each wave condition and it significantly influences power output. These findings provide essential insights for designing MPPT algorithms and enhancing power efficiency for PA-WECs.

Keywords: wave energy converter, point absorber, maximum power point tracking.

* Corresponding author, e-mail: wyhsu@mail.ntou.edu.tw

Received July 7, 2024, accepted October 22, 2024.

1 INTRODUCTION

In 2022, the National Development Council officially published "Taiwan's Pathway to Net-Zero Emissions in 2050," outlining the actionable steps to achieve net-zero emissions by 2050 (National Development Council, 2022). Ocean energy was selected as an innovative energy and included in 12 key strategies. During decarbonization-energy meetings in 2022, the potential of ocean energy was evaluated, revealing that Taiwan could generate several gigawatts (GW) of clean power from this source. The short-term goal is to deploy ocean energy demonstration units ranging from 0 to 0.1 megawatts (MW) by 2025, with plans to establish demonstration power plants of 0.1 to 1.0 MW by 2030. To facilitate this energy transition, the Ministry of Economic Affairs announced an ocean energy feed-in tariff of 7.32 New Taiwan Dollars (NTD) per kilowatt-hour in 2022. Several industry stakeholders have conducted feasibility studies and environmental assessments to support these efforts.

Taiwan has significant potential for various ocean energies, including wave energy, tidal currents, ocean currents, and temperature gradient energy. For instance, Chang et al. (2021) assessed Taiwan's wave energy potential using the WAVEWATCH III model (NWW3) from the National Oceanic and Atmospheric Administration (NOAA) of the United States. The model incorporated wind field data from the reanalysis wind field (CFSv2) by the National Centers for Environmental Prediction (NCEP). To balance computational efficiency and accuracy, a multi-grid approach was applied. The computational grid employed a three-layer nested structure, with resolution ranging from 0.25 degrees (approximately 27.76 km latitude and 21.03-27.83 km longitude) in the Northwest Pacific to 5 km in local coastal areas. This methodology provided insights into the distribution of wave energy potential, crucial for subsequent evaluations. Figure 1 illustrates that wave energy is relatively low (below 6 kW/m) in the western and southwestern seas of Taiwan, increasing in the eastern coastal areas. Higher wave energy levels (greater than 10 kW/m) are observed in the Taiwan Strait west of Penghu, the Bashi Channel, and offshore areas northeast and east of Taiwan.

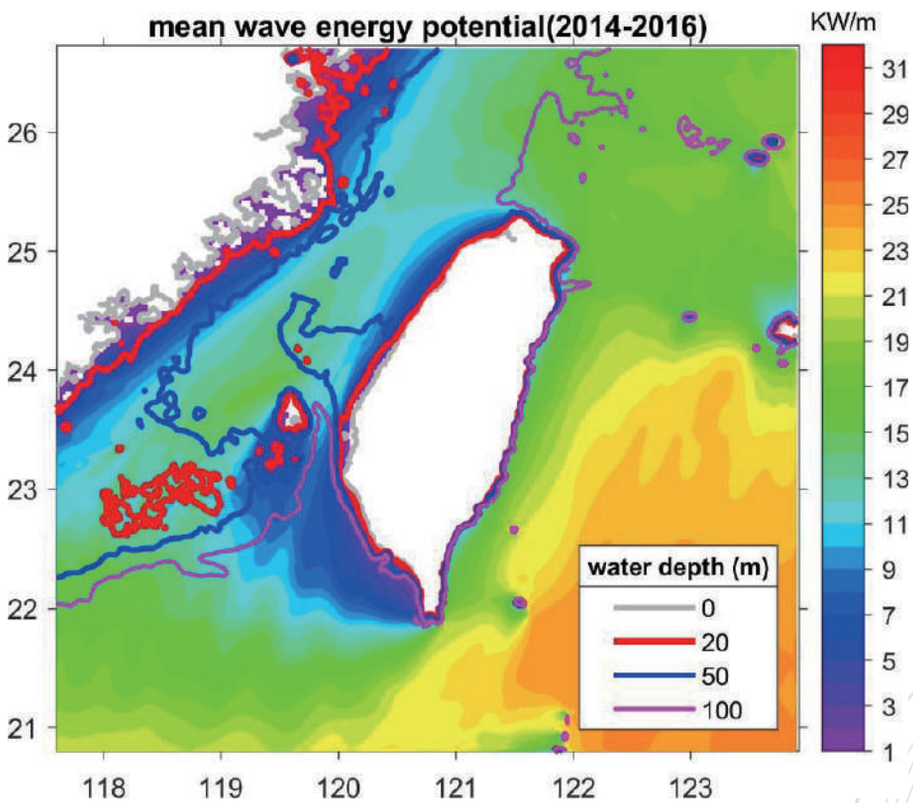

Figure 1. Mean wave energy potential of Taiwan. The simulated period ranges from 2014 to 2016. The wave water of 0, 20, 50 and 100 m is indicated as different color lines.

Marine Research of the National Academy of Marine Research
DOI: 10.29677/MR.202412_4(2).0002

To assess the suitability of wave energy converters (WECs) for the northeast waters of Taiwan, a comprehensive review of globally applicable WEC types was conducted (Lehmann et al., 2017). The analysis revealed that most WEC designs are optimized for offshore conditions, particularly in deeper waters, leading to a higher prevalence of floating systems. Among offshore WECs, point absorbers (PA), and attenuators collectively constitute approximately 63-64% of the total, with oscillating wave surge converters (OWSC) comprising 19%, and oscillating water columns (OWC) accounting for 7%. The predominant power take-off (PTO) systems employed are hydraulic systems, followed by direct drive systems. The efficiency of WECs in converting wave energy offshore hinges significantly on their resonance effect and PTO system. Resonance is influenced by parameters such as the structure's shape, size, and mass. Typically, resonance is minimized in engineering to prevent structural damage. However, WECs operate differently, aiming to maximize motion within safe limits to capture more energy. Achieving resonance depends on design factors like inertia and restoring force (Henderson, 2006; Oskamp & Özkan-Haller, 2012; Koh et al., 2015). Furthermore, the efficiency of WECs is heavily dependent on their PTO system, which converts wave-induced motion into electrical power. Theoretical studies (Mei, 1976) suggest that the energy absorbed by the PTO equals to the energy transmitted through the WEC's motion, achieving optimal efficiency under specific wave conditions (symmetric or asymmetric).

Regarding the development of wave energy converters (WECs) over the past decade in Taiwan, the Industrial Technology Research Institute (ITRI) has focused on point-absorber (PA) WECs. Figure 2 provides an overview of the research progression. Since 2011, the first PA-WEC was developed and tested in the wave flume (1-kW) and followed by the prototype testing with a 20-kW unit in 2015. Unfortunately, the prototype suffered damage and sank during Typhoon Dujuan in 2015. The extreme waves, reaching 16 m in wave height, damaged the steel structure of the wave-stabilizing plate beneath the PA-WEC. After 2017, the ITRI changed the design to miniaturize the size of the PA-WEC in order to reduce wave impact from extreme waves.

This paper focuses on the third-generation point-absorber WEC, in which the drive train and PTO systems were integrated in the floater. A wave-to-wire model based on the ANSYS AQWA software is presented in Section 2. Section 3 presents the simulation results of different PTO damping and Section 4 shows the measurements of maximum power output in the scaled experiment. Lastly, the conclusions are given in Section 5.

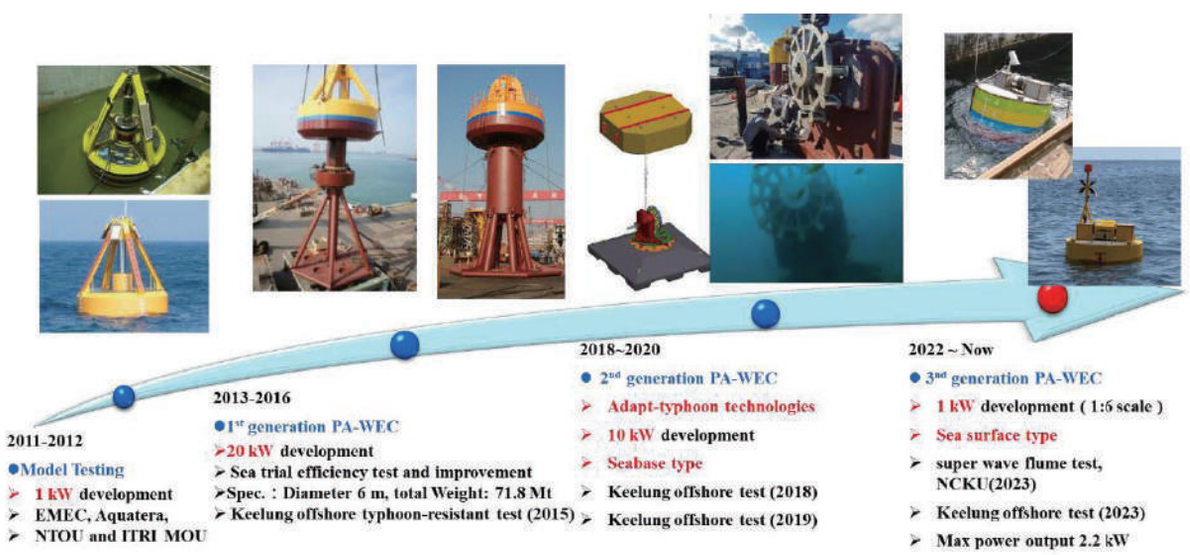

Figure 2. PA-WEC development roadmap of the ITRI from 2011 to the present.

Marine Research of the National Academy of Marine Research
DOI: 10.29677/MR.202412_4(2).0002

2 MODEL SIMULATION OF PA-WECs

PA-WECs aim to convert the hydrodynamic force into a winch PTO system via a floating device. The winch PTO operates using a rope system, with one end statically anchored on the sea bottom. The floater is designed to harness the surge/sway and heave motions as the primary power absorption. A pre-tension force device is applied to avoid slack conditions for the driving rope. The PA-WEC is composed of four main components: floating buoy, restoring device, alternator system, and power system, as shown in Figure 3. The prototype of the PA-WEC buoy has a diameter of 9 m. The scale-down ratio 1:6 was selected in this study by using the Froude number. As a result, the buoy has a diameter of 1.5 m. The dimensions of the PA-WEC are listed in Table 1.

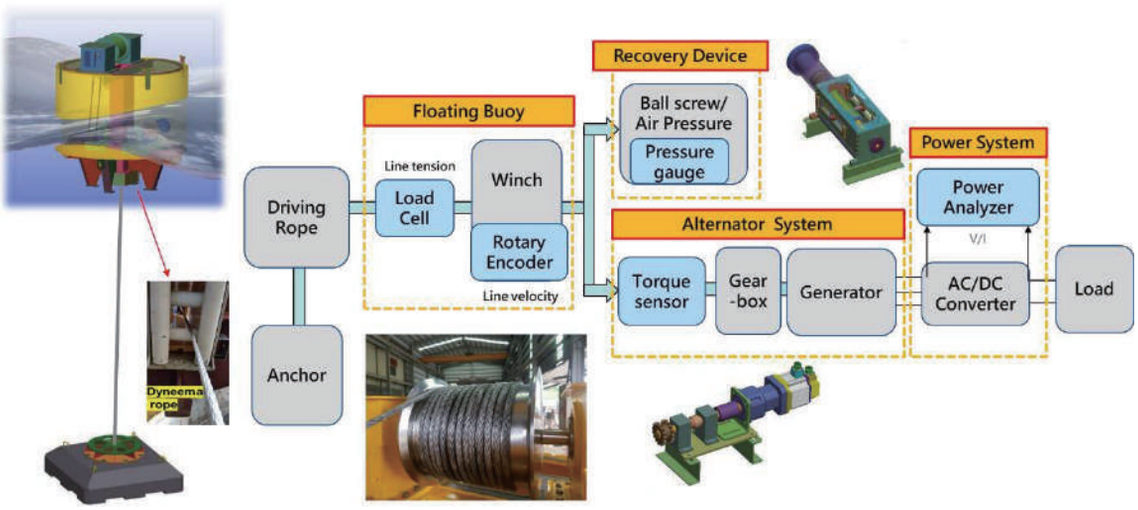

Figure 3. Sketch flowchart of the PA-WEC's drivetrain.

Table 1. Dimensions and weight of the PA-WEC.

	Unit	Value
Diameter	mm	1,500
Height	mm	1,000
Draft	mm	700
Total weight	kg	1,100

Marine Research of the National Academy of Marine Research
DOI: 10.29677/MR.202412_4(2).0002

The ANSYS AQWA software was used to establish a wave-to-wire model for the PA-WEC. The six degrees of freedom (DOF) of the buoy, rope forces, rope pay-out and pull-in from the winch, rope velocity, and power output under different PTO dampings were simulated. Figure 4 presents the simulation framework of the wave-to-wire model. The top panel of Figure 4 calculates the wave forcing components from a frequency-domain potential flow Boundary Element Method (BEM) solver. The frequency-domain hydrodynamic coefficients are converted to time-domain hydrodynamic forces using linear wave theory, which assumes the waves are the sum of incident, radiated, and diffracted wave components. The dynamic response of the system is calculated by solving the WEC system equations of motion. The equation of motion for a floating body regarding its center of gravity can be given as Eq. (1).

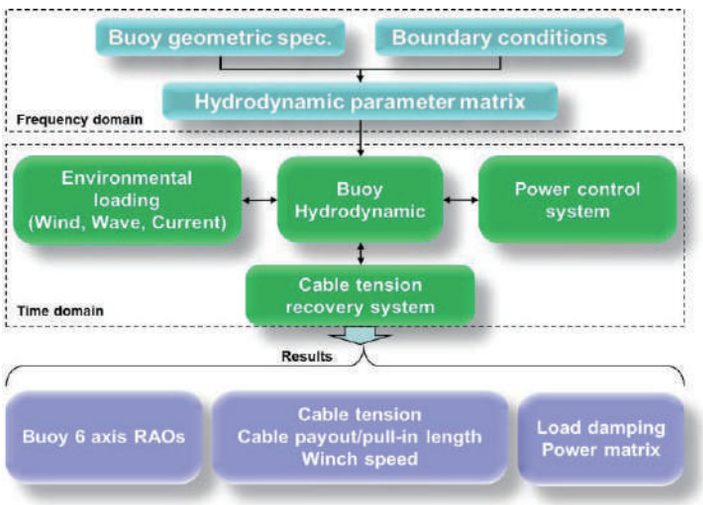

Figure 4. Framework of the wave-to-wire model.

Equation 1 describes the motion for a floating body regarding its center of gravity. The viscous effects of seawater are neglected, and the wetted body surface is assumed to be constant, without considering phenomena such as breaking waves or overtopping. This approach aligns with the small-amplitude wave theory.

$$m\begin{bmatrix} a_x \\ a_y \\ a_z \end{bmatrix} = f_{exc} + f_{rad} + f_B + f_{PTO} \tag{1}$$

According to the potential flow theory, the excitation force *fexc* acts on a rigid floating body due to incoming waves. The mass of the rigid floating body is denoted by m, and a_i represents the acceleration it experiences. The radiation force f_{rad}, which arises from the oscillations of the floating body, modifies the surrounding flow field in a quiescent water surface. This relationship is expressed as follows:

$$f_{rad} = -m_a\begin{bmatrix} a_x \\ a_y \\ a_z \end{bmatrix} - R(\omega)\begin{bmatrix} v_x \\ v_y \\ v_z \end{bmatrix} \tag{2}$$

The *added mass* m_a represents the additional mass a system acquires due to its acceleration or deceleration. When a body undergoes unsteady motion (i.e., $dU/dt \neq 0$), it displaces a volume of the surrounding fluid, effectively increasing its mass. The damping coefficient $R(\omega)$ accounts for the resistance to motion caused by the surrounding fluid, quantifying the damping effect on the system due to fluid interactions.

Marine Research of the National Academy of Marine Research
DOI: 10.29677/MR.202412_4(2).0002

Furthermore, assuming that the wetted area S between the floating body and the stationary water surface is constant, the net buoyancy restoring force f_B from water can be expressed as follows:

$$f_B = -\rho g S \begin{bmatrix} x \\ y \\ z \end{bmatrix} \tag{3}$$

When the buoy extracts energy during the phase of wave trough to wave crest, the dyneema rope on the winch will pay out, and the force is the summation of restoring force and alternator load. On the other hand, the winch will haul in from the phase of wave crest to wave trough, and only the restoring force exists. Therefore, the PTO force (f_{PTO}) can be can be expressed as follows:

$$f_{PTO} = -\left(R_{PTO} \begin{bmatrix} v_x \\ v_y \\ v_z \end{bmatrix} + f_{preT} \right) \tag{4}$$

PTO damping coefficient R_{PTO} is determined from the loading resistance of the alternator, while the pretension force, denoted as f_{preT}, is driven by the restoring device.

The governing equation of the PA-WEC motion can be obtained as follows when the winch rotates in the payout direction (winch speed v_S>0):

$$(m + m_a) \begin{bmatrix} a_x \\ a_y \\ a_z \end{bmatrix} + [R(\omega) + R_{PTO}] \begin{bmatrix} v_x \\ v_y \\ v_z \end{bmatrix} + \rho g S \begin{bmatrix} x \\ y \\ z \end{bmatrix} + f_{preT} \begin{bmatrix} x \\ y \\ z \end{bmatrix} = f_{exc} \begin{bmatrix} x \\ y \\ z \end{bmatrix} \tag{5}$$

The winch is hauled in (winch speed $v_S \leqq 0$) due to the pretension force after the waves have passed, and the loading from the generator system also vanishes (R_{PTO}=0). The governing equation can be rewritten as follows:

$$(m + m_a) \begin{bmatrix} a_x \\ a_y \\ a_z \end{bmatrix} + R(\omega) \begin{bmatrix} v_x \\ v_y \\ v_z \end{bmatrix} + \rho g S \begin{bmatrix} x \\ y \\ z \end{bmatrix} + f_{preT} \begin{bmatrix} x \\ y \\ z \end{bmatrix} = f_{exc} \begin{bmatrix} x \\ y \\ z \end{bmatrix} \tag{6}$$

3 NUMERICAL RESULTS

Figure 5 illustrates the characteristics of rope tension and winch line velocity under various PTO damping values, ranging from 2,500 to 20,000 N·s·m^{-1}. The increased PTO damping results in a higher force acting on the Dyneema rope, while subsequently causes a reduction on the floater motion and the winch speed. Therefore, from the perspective of maximizing power generation (rope tension × rope velocity), it is necessary to find optimal damping for varying wave conditions.

Marine Research of the National Academy of Marine Research
DOI: 10.29677/MR.202412_4(2).0002

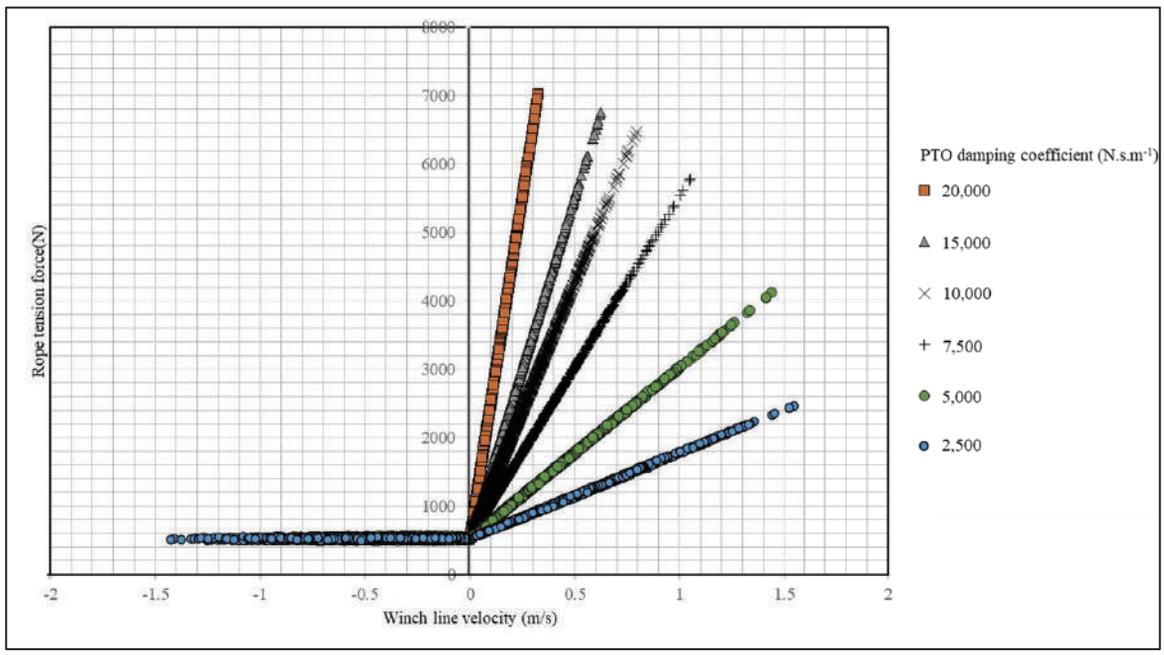

Figure 5. Characteristics of the winch line speed and rope tension under different PTO damping coefficients.

For instance, when the simulated PTO damping coefficient was set at 5,000 N·s·m^{-1} and the JONSWAP spectrum (γ = 2.2) had a significant wave height (H_s) of 0.8 m, and a peak period (T_p) of 4 s was applied, the PA-WEC could generate an average output of 420 W and a maximum output of 1900 W, as shown in Figure 6. If higher or lower PTO dampings were applied, the average and maximum power all decreased, as shown in Figure 7. As a result, the PTO damping coefficient of 5,000 N·s·m^{-1} represents the optimal PTO damping coefficient for this wave condition. Following the same simulation algorithm, various PTO damping settings were adjusted for different wave conditions. A total of 12 wave conditions were simulated, and their average power outputs were plotted in Figure 8. This method allowed us to estimate the range of PTO damping and predict power generation before conducting the tank tests. All simulation results further indicate that load damping can achieve an acceptable power output within the range of 4,000 to 6,000 N·s·m^{-1}, suggesting that this range is suitable for practical adjustment, as shown in Figure 7.

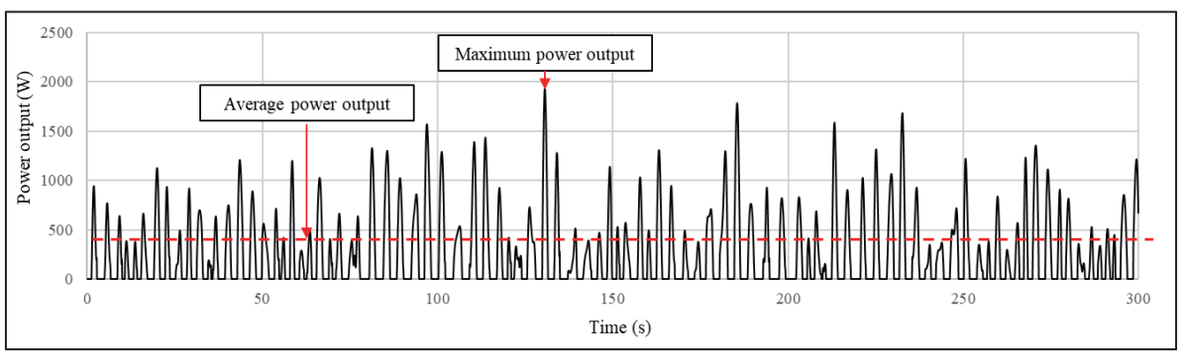

Figure 6. Time series power output of simulated PA-WEC under JONSWAP wave conditions (γ = 2.2, H_s= 0.8 m and peak period T_p= 4 s, PTO damping= 5,000 N·s·m^{-1}).

DOI: 10.29677/MR.202412_4(2).0002

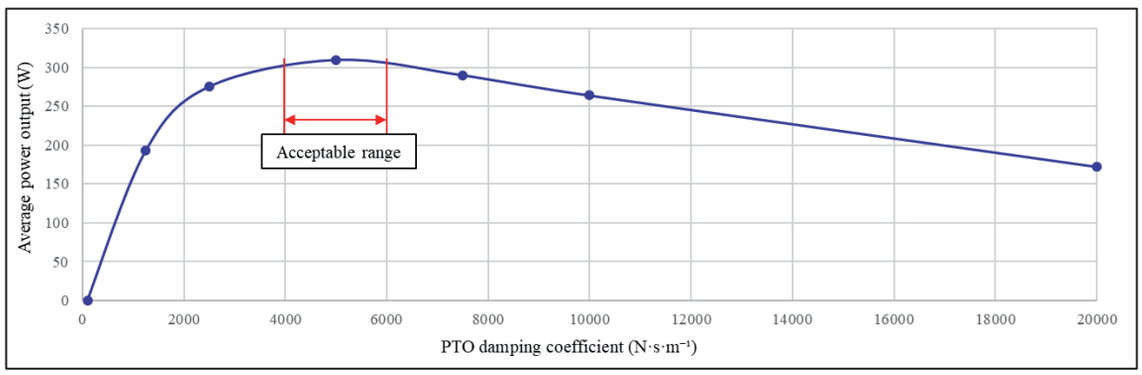

Figure 7. Averaged power output under different PTO dampings under JONSWAP wave conditions (γ = 2.2, H_s= 0.8 m and peak period T_p= 4 s).

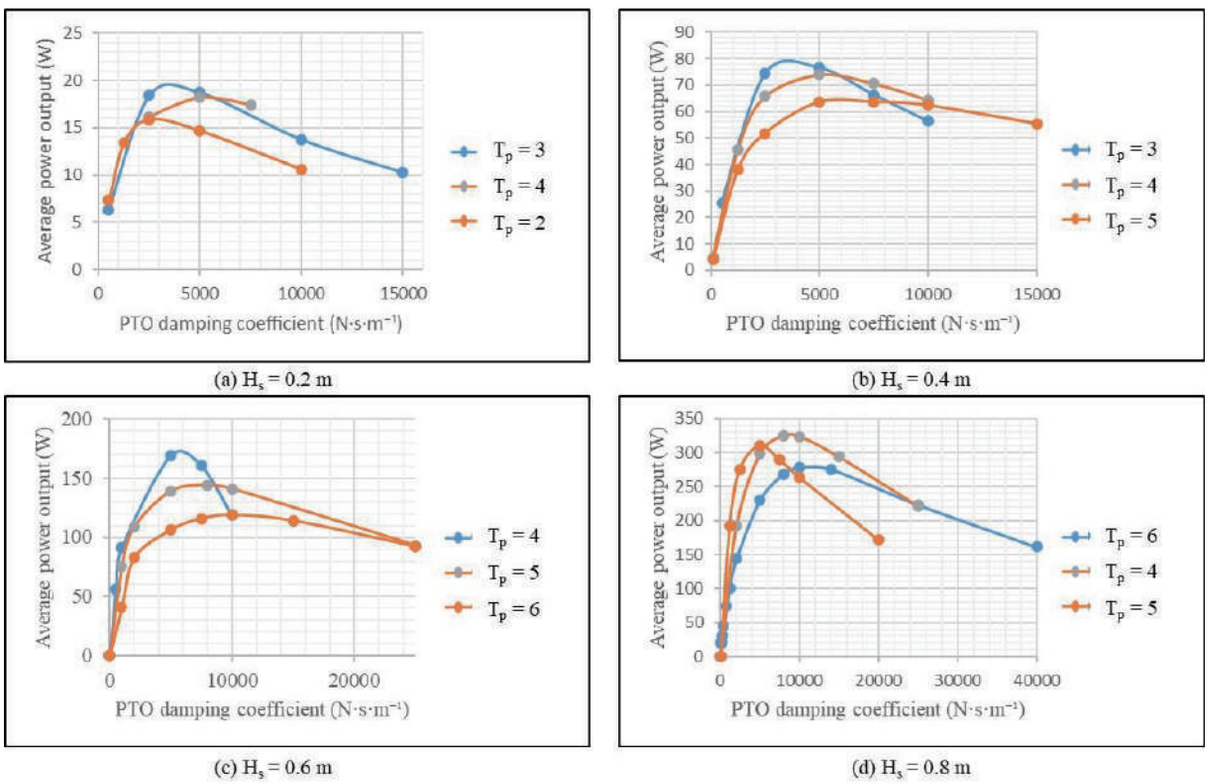

Figure 8. Simulated average power output of PA-WEC under different JONSWAP wave conditions. The significant wave height ranges from 0.2 to 0.8 m and peak period ranges from 2 to 6 s.

Marine Research of the National Academy of Marine Research
DOI: 10.29677/MR.202412_4(2).0002

4 EXPERIMENTAL RESULTS AND DISCUSSION

To validate the simulated power output of the PA-WEC, we conducted a large-scale experiment with a 1:6 Froude scale in the wave flume (length: 300 m; width: 5 m; depth: 5.2 m) at the Tainan Hydraulics Laboratory, National Cheng Kung University in Taiwan. JONSWAP waves were generated using a computer-controlled, hydraulically driven, dry-back, piston-type programmable wavemaker situated at one end of the flume. Figure 9 depicts a schematic diagram of the experimental setup, configuration, and photos of the setup during the experiment.

Surface elevations were measured using capacitance-type wave gauges mounted along a sidewall of the wave flume. Rope tension and six-axis degrees of freedom were measured using a load cell and an inertial measurement unit (IMU), respectively. Each test lasted 10 minutes, during which all sensors recorded data simultaneously at a sampling rate of 10 Hz using a data logger system. The static water depth was maintained at 3 m. Figure 10 shows the test of the PA-WEC in the wave flume under irregular wave conditions.

The wave conditions used in the wave experiment were based on the joint probability distribution of wave height and period observed at the NTOU test site (Chen et al., 2020). The site is located in the marine area between the outer side of the College of Engineering's seawall at Ocean University and Keelung Islet, encompassing two testing zones: one near the seawall of the College of Engineering for wave testing and another above the sea shelf near Keelung Islet for tidal energy testing. The water depth in the wave testing area is up to 40 meters. Figure 11 illustrates the cumulative wave energy distribution, in which the highest cumulative wave energy occurs at a wave height of 2.5 meters and a period of 8.5 seconds. The annual incident wave energy is 3,641 kWh/m at this weather condition. To assess the power generation capacity of the scaled PA-WEC in the wave flume, we selected test conditions within a period range of 2 to 6 seconds (equivalent to 4.9 to 14.7 seconds in full scale) and wave heights from 0.2 to 0.8 meters (equivalent to 1.2 to 4.8 meters at full scale).

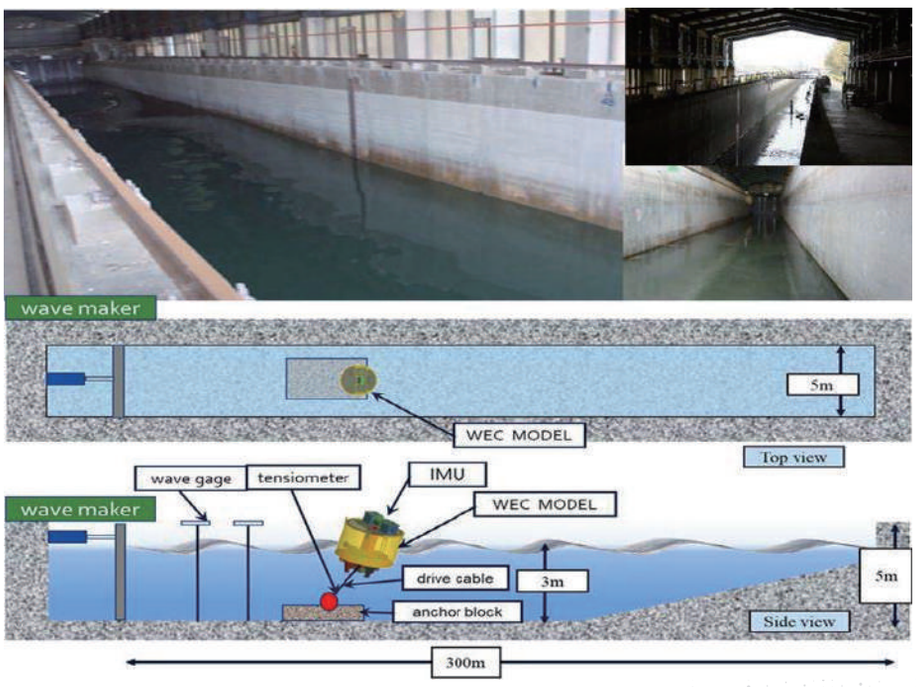

Figure 9. Experiment facility configuration.

Marine Research of the National Academy of Marine Research
DOI: 10.29677/MR.202412_4(2).0002

Figure 10. Photo of the wave tank test under irregular wave conditions.

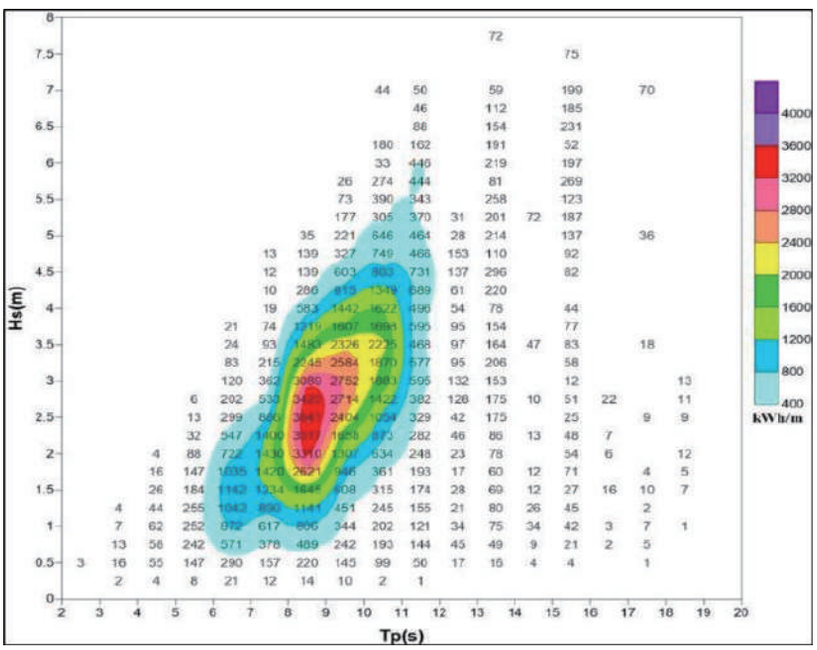

Figure 11. Joint probability distribution of cumulative wave energy distribution at the test site of National Taiwan Ocean University.

Marine Research of the National Academy of Marine Research
DOI: 10.29677/MR.202412_4(2).0002

During the experiments, the optimal PTO dampings were adjusted by changing the electrical resistance loads. For each wave condition, the lightest resistance load started at 36 ohms and the load was gradually increased until the maximum power output of the PA-WEC was revealed. The measurements of incident wave energy, loading resistance, loading voltage, loading current, average/maximum power output, and power efficiency for a significant wave height of 0.56 m and peak wave period of 3.13 sec are listed in Table 2.

Table 2. Measurements of power outputs under different resistance loads.

H_s	0.56 m						
T_p	3.13 s						
Incident Wave Energy	0.67 kW						
Test Result	No.	Loading Resistance (ohm)	Average Loading Voltage (V)	Average Loading Current (A)	Average Power Output (W)	Maximum Instantaneous Power Output (W)	Average Efficiency (%)
	1	36	27.65	0.78	67.04	1,303.62	9.94
	2	27	25.29	0.94	74.66	1,411.89	11.07
	3	18	21.81	1.21	82.38	1,537.19	12.22
	4	9	16.07	1.79	87.28	1,482.87	12.94
	5	4.5	10.48	2.28	70.27	985.98	10.42

A total of 12 wave conditions were tested, and 5 resistance loads were applied for each wave condition. Finally, the power matrix was plotted under different incident wave energies and resistance loads, as shown in Figure 12. The incident wave energy was calculated as $0.458H_s^2T_p$ (Shuichi, 2015). The power matrix visualizes the path of the maximum power point tracking (MPPT) curve.

On the other hand, power efficiency, defined as the net power generation (kW) divided by the incident wave energy per unit of capture width (kW), was analyzed to produce the power efficiency map, as shown in Figure 13. The areas of high efficiency correspond to wave conditions with a period of 2.13 seconds, which matches the resonant period (obtained from the ANSYS AQWA software) of heave motion for the PA-WEC. Because wave energy is inherently intermittent across different time scales, power efficiency can range from 2% to 15%. Figure 13 highlights the critical importance of MPPT for wave energy systems.

DOI: 10.29677/MR.202412_4(2).0002

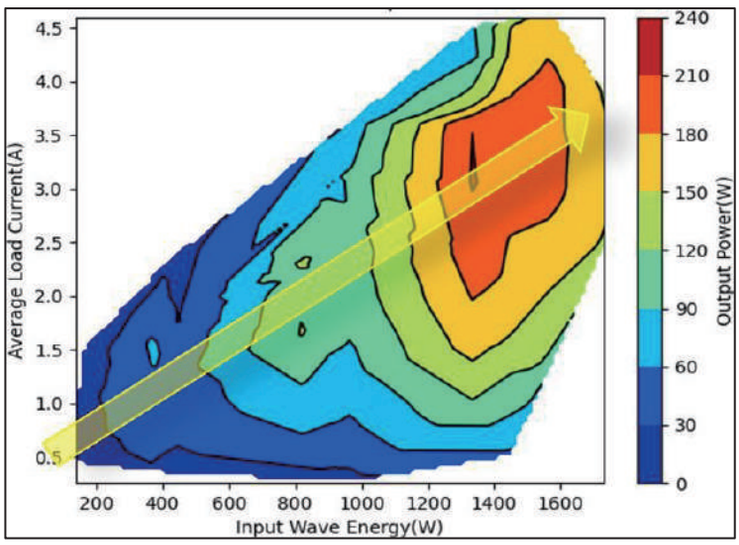

Figure 12. Power matrix and optimal control path of load current for the PA-WEC under irregular wave conditions.

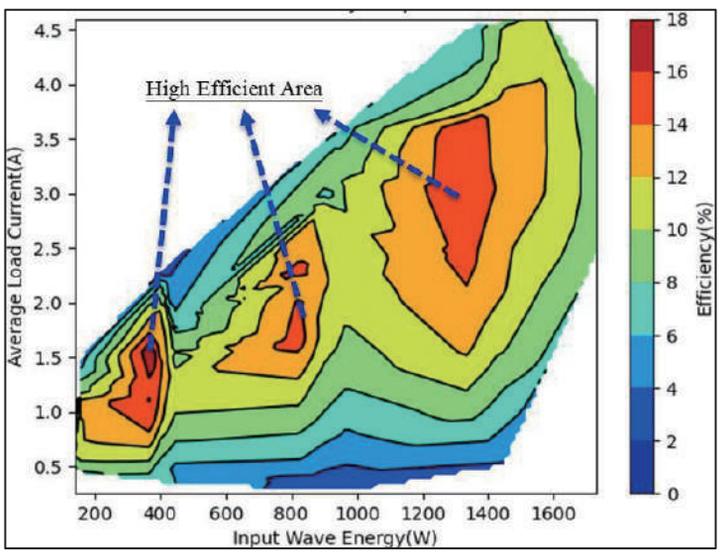

Figure 13. Efficiency matrix for the PA-WEC under irregular wave conditions.

Marine Research of the National Academy of Marine Research
DOI: 10.29677/MR.202412_4(2).0002

5 CONCLUSIONS

This study establishes an effective approach for designing the MPPT algorithm for a point-absorber wave energy converter system. Both numerical simulations and experimental results revealed that optimal PTO damping values, ranging between 4,000 and 6,000 $N \cdot s \cdot m^{-1}$, significantly influence the power output of the PA-WEC. By applying these damping coefficients, power output was maximized, aligning well with the observed performance during physical experiments. Additionally, the experimental results confirmed the accuracy of the numerical model, which demonstrated the ability to predict power generation under varying wave conditions. These findings are critical for developing MPPT strategies and advancing the design of future PA-WEC systems to improve power efficiency and performance under real sea conditions. The study also highlights the potential that wave energy has to contribute significantly to Taiwan's renewable energy goals, especially in its pathway to achieving net-zero emissions by 2050.

ACKNOWLEDGEMENTS

The authors wish to thank the Energy Administration, Ministry of Economic Affairs, R.O.C., for providing financial assistance for this work (113-D0311).

REFERENCES

Chang, Y. C., Chou, R. C., Chen, D. W., Lin, C. C., Tseng, C. C., & Chen, G. Z. (2021). Assessment of wave power generation technology for the waters of Taiwan's Northeast corner. *Journal of Taiwan Power Company, 895,* 1-16. https://www.taipower.com.tw/_upload/86/20230322172912341 85.pdf

Chen, H. Z., Ciou, J. Y., Tzang, S. Y., Lee, Y. H., & Chen, J. H. (2020) Wave energy resources in the Ocean Energy Testing Field in Keelung – buoy station. *Proceedings of the 20th Ocean Engineering Conference*, 682-687.

Henderson, R. (2006). Design, simulation, and testing of a novel hydraulic power take-off system for the Pelamis wave energy converter. *Renew. Energy, 31*(2), 271-283. https://doi.org/10.1016/j.renene.2005.08.021

Koh, H. J., Ruy, W. S., Cho, I. H., & Kweon, H. M. (2015) Multi-objective optimum design of a buoy for the resonant-type wave energy converter. *Journal of Marine Science and Technology, 20,* 53-63. https://doi.org/10.1007/s00773-014-0268-z

Lehmann, M., Karimpour, F., Goudey, C. A., Jacobson, P. T., & Alam, M. R. (2017) Ocean wave energy in the United States: Current status and future perspectives. *Renewable and Sustainable Energy Reviews, 74,* 1300-1313. https://doi.org/10.1016/j.rser.2016.11.101

Mei, C. C. (1976) Power extraction from water waves. *Journal of Ship Research, 20*(2), 63-66. https://doi.org/10.5957/jsr.1976.20.2.63

Nagata, S. (2015). Chapter 4: Wave power. In H. Kondo (Ed.), *Ocean energy utilization technology* (2nd ed., pp.49-104). Morikita Publishing. (in Japanese) https://www.morikita.co.jp/books/mid/091462

National Development Council (2022). *Taiwan's pathway to Net-Zero Emissions in 2050.* https://www.ndc.gov.tw/en/Content_List.aspx?n=B154724D802DC488

Oskamp, J. A., & Özkan-Haller, H. T. (2012) Power calculations for a passively tuned point absorber wave energy converter on the Oregon coast. *Renewable Energy, 45*, 72-77. https://doi.org/10.1016/j.renene.2012.02.004